Atmospheric Ice-Nucleating Particles in the Dusty Tropical Atlantic

H. C. Price[1,2,3] ID, K. J. Baustian[1], J. B. McQuaid[1] ID, A. Blyth[1,3] ID, K. N. Bower[4] ID, T. Choularton[4] ID, R. J. Cotton[5], Z. Cui[1] ID, P. R. Field[1,5], M. Gallagher[4] ID, R. Hawker[1], A. Merrington[1], A. Miltenberger[1] ID, R. R. Neely III[1,3] ID, S. T. Parker[6], P. D. Rosenberg[1] ID, J. W. Taylor[4] ID, J. Trembath[2], J. Vergara-Temprado[1] ID, T. F. Whale[1] ID, T. W. Wilson[1] ID, G. Young[4,7], and B. J. Murray[1] ID

[1]School of Earth and Environment, University of Leeds, Leeds, UK, [2]Facility for Airborne Atmospheric Measurements, Cranfield, UK, [3]National Centre for Atmospheric Science (NCAS), University of Leeds, Leeds, UK, [4]Centre for Atmospheric Science, School of Earth and Environmental Sciences, University of Manchester, Manchester, UK, [5]UK Met Office, Exeter, UK, [6]Defence Science and Technology Laboratory, Salisbury, UK, [7]British Antarctic Survey, Cambridge, UK

Abstract Desert dust is one of the most important atmospheric ice-nucleating aerosol species around the globe. However, there have been very few measurements of ice-nucleating particle (INP) concentrations in dusty air close to desert sources. In this study we report the concentration of INPs in dust laden air over the tropical Atlantic within a few days' transport of one of the world's most important atmospheric sources of desert dust, the Sahara. These measurements were performed as part of the Ice in Clouds Experiment-Dust campaign based in Cape Verde, during August 2015. INP concentrations active in the immersion mode, determined using a droplet-on-filter technique, ranged from around 10^2 m^{-3} at −12°C to around 10^5 m^{-3} at −23°C. There is about 2 orders of magnitude variability in INP concentration for a particular temperature, which is determined largely by the variability in atmospheric dust loading. These measurements were made at altitudes from 30 to 3,500 m in air containing a range of dust loadings. The ice active site density (n_s) for desert dust dominated aerosol derived from our measurements agrees with several laboratory-based parameterizations for ice nucleation by desert dust within 1 to 2 orders of magnitude. The small variability in n_s values determined from our measurements (within about 1 order of magnitude) is striking given that the back trajectory analysis suggests that the sources of dust were geographically diverse. This is consistent with previous work, which indicates that desert dust's ice-nucleating activity is only weakly dependent on source.

1. Introduction

The formation of ice in supercooled clouds is of fundamental importance for the formation of precipitation, as well as cloud lifetime and radiative properties (McCoy et al., 2015; Tan et al., 2016). Mineral dust originating from the world's arid regions is one of the most important aerosol types for triggering ice nucleation, not only in locations close to deserts but also thousands of kilometers from source regions (Atkinson et al., 2013; Baustian et al., 2012; DeMott et al., 2003; Hoose et al., 2010; Wiacek et al., 2010). Of the various arid source regions, the Sahara is the largest single source (Formenti et al., 2011; Prospero et al., 2002; Ridley et al., 2012) with ~100 Tg of dust per year exported to the tropical Atlantic and beyond (Kaufman et al., 2005).

Mineral dust particles can serve as ice-nucleating particles (INPs), even when transported far from source and after interaction with other atmospheric constituents. Aircraft observations have shown that INP concentrations correlate with dust concentrations in dust plumes transported over Florida (DeMott et al., 2003), and measured INP concentrations in dust plumes at mountain top atmospheric observatories were also found to correlate with dust concentrations (Boose, Kanji, et al., 2016; Boose, Sierau, et al., 2016; Chou et al., 2011; Klein et al., 2010). There is a propensity to find mineral dust particles within cloud ice crystals indicating that mineral dust nucleated those ice crystals (Cziczo et al., 2013; Kamphus et al., 2010; Pratt et al., 2009; Twohy, 2014). Similarly, experiments where atmospheric aerosol samples were artificially exposed to supersaturated conditions, at temperatures from −63 to −43°C (Baustian et al., 2012) and from −50 to −15°C (Richardson et al., 2007), also suggest that mineral dust preferentially nucleates ice relative to other aerosol types.

Laboratory studies have been used to quantify the efficiency with which soil samples collected in desert regions nucleate ice (DeMott, Prenni, et al., 2015; Niemand et al., 2012). Desert dusts from diverse arid

sources have been shown to nucleate ice with comparable efficiency (Boose, Welti, et al., 2016; Kaufmann et al., 2016; Niemand et al., 2012), which may indicate that there is a common component of desert dusts that controls its ice-nucleating ability (Atkinson et al., 2013). Mineral dust from deserts is made up of a variety of minerals (Glaccum & Prospero, 1980; Murray et al., 2012), and experiments with specific minerals have shown that the potassium feldspars (K-feldspars) are much more effective at nucleating ice than other tested minerals in desert dusts across the mixed phase-cloud temperature regime (Atkinson et al., 2013; Augustin-Bauditz et al., 2014; Harrison et al., 2016; Kaufmann et al., 2016; Niedermeier et al., 2015; Wex et al., 2014; Whale et al., 2017; Zolles et al., 2015).

The ice-nucleating efficiency of desert dust samples from the ground (i.e., desert soils) and their mineral components have been used to determine the concentration of INPs in models (Atkinson et al., 2013; Hoose et al., 2010; Niemand et al., 2012; Vergara-Temprado et al., 2017), but very few measurements of the ice-nucleating ability of atmospheric aerosol dominated by desert dust have been made within a few days' transport over the Eastern Atlantic from source regions (Boose, Sierau, et al., 2016; Conen et al., 2015). Sampling atmospheric dust is also important because airborne desert dust is not pure mineral dust. The dust particles contain other materials from the source regions such as biological material and salt residues, which may also interact with trace gases and other aerosol in the atmosphere. Desert dust is subject to a range of chemical and physical processes, which are challenging to simulate in the laboratory, such as the saltation process and chemical weathering both on the ground and in the atmosphere. In fact, a recent study concluded that desert dust that had been transported through the air and then sampled generally had a lower activity than desert dust sampled directly from the surface (Boose, Welti, et al., 2016). Hence, it is important that we test our ability to predict the ice-nucleating ability of desert dust dominated aerosol based on idealized laboratory-based parameterizations against in situ measurements.

In order to make measurements of the INP spectrum (i.e., the INP concentration as a function of ice-activation temperature) from an aircraft, we use a technique originally described and used by Schnell (1982). This technique involves collecting aerosol particles onto filters via inlets located outside the boundary layer of an aircraft and then using a droplet freeze assay to quantify the concentration of INPs on the filter. This assay involves placing an array of ultrapure water droplets onto the filters in order to quantify the concentration of airborne INP particles as a function of activation temperature. Here we present the methodology and report data collected during the August 2015 ICE-D (Ice in Clouds Experiment-Dust) field campaign based in Praia, Cape Verde (14.9°N, 23.5°W). We go on to compare the INP concentration measurements, in combination with the aerosol size distribution, with several literature parameterizations for ice nucleation by desert dust.

2. Materials and Methods

2.1. The ICE-D Study Region

The ICE-D field campaign took place in the region around the Cape Verde archipelago in August 2015. This region is strongly impacted by dust from sources across North Africa with the dust layers typically below 5 km. As part of the campaign, the UK's Facility for Airborne Atmospheric Measurements (FAAM) BAe-146 research aircraft was used to sample and characterize cloud and aerosol layers. The aircraft was based out of Praia on the island of Santiago and flights focused on the oceanic region around Cape Verde with flights as far away as the Canary Islands. The flight tracks and location of filter sampling is shown in Figure 1.

2.2. Sample Collection

Onboard the FAAM research aircraft, filter samples were collected using the two parallel filter inlets on the port side of the aircraft. This inlet system was in use on the C-130 aircraft before being installed on the FAAM BAe-146 aircraft and has been used in the past to sample fine and coarse mode atmospheric aerosol (e.g., Andreae et al., 2000; Formenti et al., 2008; Young et al., 2016). The aluminum nozzle inlets are positioned outside of the aircraft boundary layer and approximately aligned with the local airflow. The inlet design was based on criteria for aircraft engine intakes in order to minimize flow separation and turbulence. A vacuum pump, aided by the ram effect of the aircraft, pulls air through the inlets, and flow volumes are measured using mass flowmeters, which report standard liters sampled (where standard temperature is taken to be 273.15 K and standard pressure 101.3529 kPa). Flow rates vary with altitude (as well as between different types of filter) with lower flow at higher altitudes due to the reduced pressure differential across the filter. At high altitude the flow rate is so reduced that it is not practical to sample for a sufficiently long duration
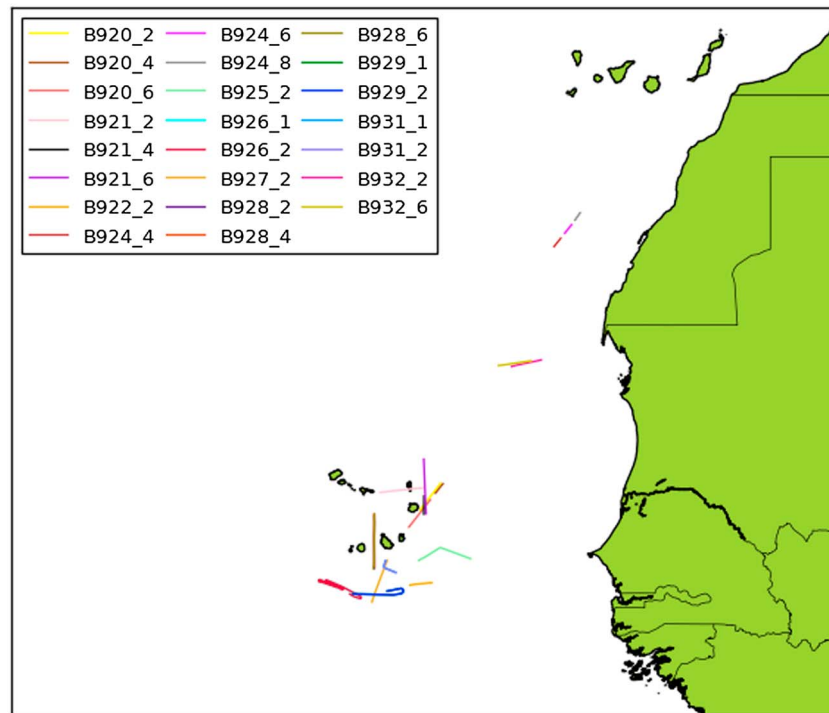
Figure 1. Track plots showing the sampling locations of each of the filters.

to collect a sample for analysis; we thus limit the measurements reported here to below 3,500 m (11,500 ft). Filter samples were only collected in the absence of clouds or precipitation. The system is equipped with a bypass line, the flow through which can be controlled independently of the main sampling line. For the sampling here, the bypass line was closed in order to maintain subisokinetic conditions and also to allow direct comparison with previous sampling (Young et al., 2016) where the bypass was closed. Sampled air passes through filter holders positioned behind the inlet. These filter holders are isolated or exposed to sample flow in-flight by using manually operated valves.

Two types of filter holders were used, one for INP concentration analysis and one for scanning electron microscope (SEM) analysis. The filter holders for the INP concentration analysis were modified for this study and are illustrated in Figure 2. The holder is designed to keep the filters as flat as possible and minimize deformation. This is done by using a 47 mm stainless steel fine mesh support screen (XX4304707, Millipore) to support the filter, with a nitrile rubber O-ring holding it in place. Sartorius polytetrafluoroethylene (PTFE) membrane filters (47 mm diameter, type-11806) with a pore size of 0.45 μm were chosen due to their hydrophobicity (and thus high contact angle for the droplet freezing assay) and their low ice-nucleating efficiency. It has been shown that similar filters collect aerosol down to 10 nm with an efficiency greater than 99% (Soo et al., 2016). It was very important to expose the shiny side of these filters, as the dull side of some filters was found to nucleate ice at temperatures up to −6°C. Flow rates through these filters on the aircraft were up to 20 standard liters per minute (sLmin^{-1}). Filters were loaded into their holders in a clean hood (where air was filtered) in the temporary laboratory in Cape Verde, and the holders and supports were cleaned in an ultrasonic bath between each use.

The filter holders for the filters for SEM analysis were the standard configuration, which has been used in the past (e.g., Young et al. (2016)). These were collected in parallel with the filters for INP analysis. Polycarbonate track etched filters with 0.4 μm pores (Whatman, Nucleopore) were used. Composition analysis was determined using a Phillips FEI XL30 Environmental Scanning Electron Microscope with Field-Emission Gun (ESEM-FEG) combined with an energy-dispersive X-ray spectroscopy system, based at the University of Manchester Williamson Research Centre. The system is described previously (Hand et al., 2010; Johnson et al., 2012). As discussed in Young et al. (2016), this technique is insensitive to carbonaceous particles due
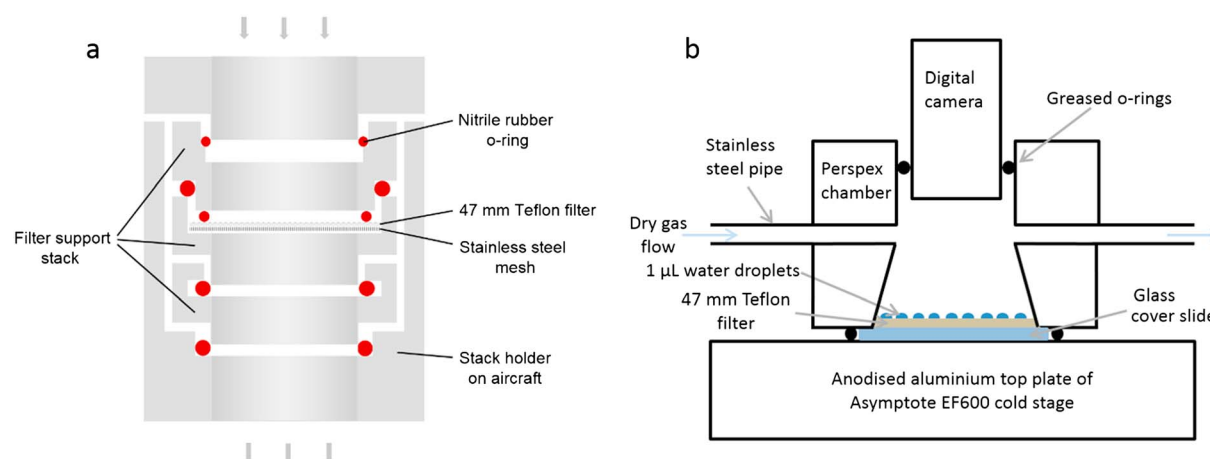
Figure 2. The filter sampling and ice-nucleating particle analysis equipment. (a) Cross section of filter holder. A 47 mm Teflon filter sits on a fine stainless steel mesh, held in place by nitrile rubber O-rings. The filter stack is designed to fit into the standard filter holders on the BAe-146 aircraft. (b) The Nucleation by Immersed Particle Instrument described by Whale et al. (2015), but adapted for use with the 47 mm filter. The filter is placed on top of a hydrophobic glass cover slide.

to interference from the substrate. In addition, any volatile materials are lost when exposed to the vacuum in the instrument.

2.3. Droplet Freezing Assay

The droplet freezing assay technique used in this study is an adaptation and combination of techniques described by Whale et al. (2015) and Schnell (1982). Briefly, 1 μL liquid droplets are cooled at constant rate of 1 K per minute by an Asymptote EF600 Stirling cooler. Their freezing is observed via a video camera while measuring the temperature of the cold stage. The fraction of droplets frozen at a particular temperature can be used to calculate the concentration of INP in each droplet (see below). In this work we use the exposed filter as a substrate, rather than a glass slide as in Whale et al. (2015). As mentioned above, hydrophobic PTFE membrane filters were used. For each droplet freezing assay, a collected filter sample was placed onto a hydrophobic glass cover slide (Ted Pella cover glass, 48 × 60 × 0.15 mm), which was held in place on the metal cold stage using silicon oil. The glass was made hydrophobic to prevent ice forming on the glass surface from the vapor. This was done using Turtle Wax ClearVue Rain Repellent solution. For each experiment, a fresh slide was prepared by coating it in ClearVue; rubbing both sides with lens cleaning tissue; rinsing with water, methanol, and chloroform; drying with zero grade nitrogen gas; and repeating. Due to the large size of the slides and filters in these experiments, the base of the chamber used to cover the droplets and hold the camera was wider than that used by Whale et al. (2015) and had a conical interior, with a base diameter of 62 mm. This enabled more droplets to be used per experiment: up to 130 1 μL droplets could be used per filter (see Figure 3), as opposed to up to ~40 used previously. When the stage temperature was below the
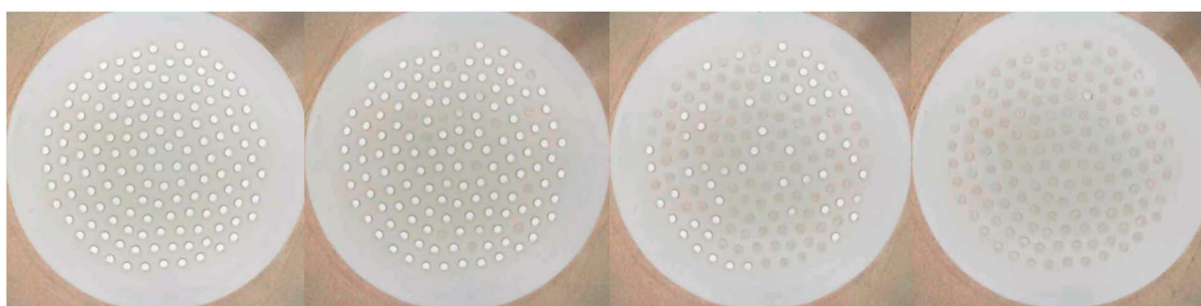

Figure 3. Stills from the video recording of a drop freeze assay experiment. At the start of the experiment all droplets are liquid (left). As the droplets are cooled, freezing events are observed, until all droplets are frozen (right). The area of the filter exposed to atmospheric aerosol can be seen by the slight discoloration of the filter; droplets are only placed in this region.
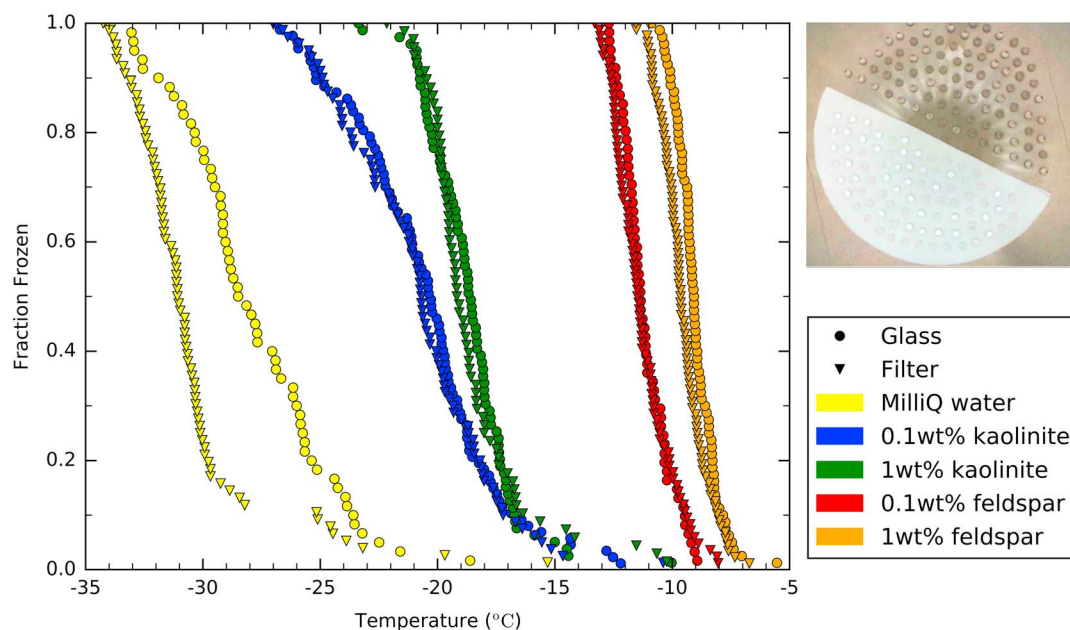
Figure 4. Experiments to assess how heat is transferred through a PTFE membrane filter on a glass slide. The uncertainty in temperature was 0.5°C. Droplets of water from the same suspension were placed on to the filter and directly onto the glass so that freezing can be observed during the same cooling cycle. There appears to be no difference in the freezing temperatures of droplets on the filter and on the glass slide, which contain ice-nucleating materials. In the case of MilliQ water, droplets on the filter freeze at lower temperatures than those on the glass slide, implying that the filter had fewer "background" heterogeneous nucleation sites than the glass.

dew point of air in the laboratory, an ~0.2 sLmin^{-1} flow of zero grade dry nitrogen was used to inhibit condensation and frost growth.

To test if the filter acted as a thermal barrier between the cold stage and the droplets, experiments were done using pure water and mineral dust suspensions in which half of the droplets in an experiment were placed on a filter and the other half were placed directly onto the glass slide (see image in Figure 4). The results of these experiments are shown in Figure 4, where it can be seen that droplets containing mineral dusts have the same freezing temperatures on both the glass slide and on the filter. The only major difference occurred for pure MilliQ (18.2 MΩ cm) water, when droplets on the filter froze at lower stage temperatures than those on the glass slide. The offset between the two sets of droplets is not constant, implying that the difference is caused not by a lack of thermal contact but by a difference in the ice-nucleating properties of the two substrates.

Filters exposed on the aircraft were prone to slight deformation at high flow rates, and care was required to ensure that each droplet was in good thermal contact with the cold stage. To assess the thermal contact, the melting of the droplets was recorded by the camera as they warmed back to room temperature after freezing. It was clear from a visual inspection of the melting pattern which droplets were in poor thermal contact with the cold stage due to a slight deformation of the filter: these droplets (usually a small fraction of the total) melted much later than the majority. These droplets, together with their immediate neighbors, were disregarded from the analysis. Most of our filters were in good thermal contact with the cold stage and only a minority required droplets to be disregarded as described. When droplets were disregarded, the reduced number of data points in the experiment is reflected in the uncertainty analysis.

Samples collected on the FAAM BAe-146 aircraft were taken to a temporary laboratory immediately after landing, and either the freezing experiment described above was done on the same day as sampling or the sample was stored at −18°C for analysis over the following days. Filters were unloaded from their holders in a clean hood (with filtered air) and placed in individual, sealed Petri dishes prior to analysis. We used HiPerSolv CHROMANORM® water in the drop freeze assays. All aircraft samples were analyzed by drop freeze assay on the island in order to avoid issues associated with transportation and long-term storage.
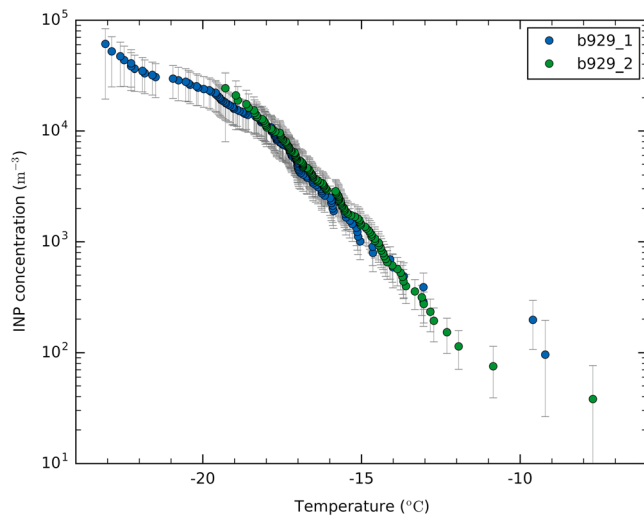
Figure 5. Measured ice-nucleating particle concentration for two filters collected simultaneously using different flow rates during flight B929.

In a drop freeze assay experiment, the number of INP per unit volume of water at a given temperature, T, is given by Vali (1971)

$$K(T) = \frac{-\ln(1 - f(T))}{V_d} \tag{1}$$

where f is the fraction of droplets frozen at temperature T and V_d is the volume of each uniformly sized droplet, 1 ± 0.1 μL. The uncertainty in $K(T)$ is determined using Monte Carlo simulations to find the Poisson sampling uncertainty (Harrison et al., 2016). $K(T)$ can be used to derive the atmospheric INP concentration with knowledge of the total flow volume and area the droplet occupied on the filter. If a filter was used to sample a volume V_a of air (measured by two Alicat MFC units onboard the aircraft), the number of INP per unit volume of air, [INP], is calculated as follows:

$$[\text{INP}](T) = \frac{K(T) V_d A_{\text{fil}}}{V_a \alpha} \tag{2}$$

where A_{fil} is the area of the filter exposed to aerosol particles and α is the area of each droplet in contact with the filter. A_{fil} was found to be 11 ± 2 cm^2 by measuring the diameter of the discolored region on filters exposed to high aerosol loadings. The α was determined to be 0.9 ± 0.1 mm^2 based on a droplet volume of 1 ± 0.1 μL and a contact angle of $126 \pm 3°$, with the assumption of a spherical cap geometry. The contact angle was measured using a contact angle goniometer: five of our exposed filters were used for these measurements, with the contact angles of five droplets on each measured using the goniometer. The uncertainty in the volume of air sampled was estimated to be 0.5 L, and uncertainties in [INP](T) were found by standard propagation of the uncertainties in each term. The uncertainty in temperature was 0.4 K (Whale et al., 2015). The concentration calculated in this way assumes that the aerosol distribution inside the aerosol sampling system is the same as outside—it ignores any size-dependent filtering of the aerosol by the inlet system, which is discussed in section 2.3.

When analyzing a filter for atmospheric INP we first conducted blank experiments in order to test the water, surfaces, and other components for contamination. Blank experiments involved placing an unexposed filter on the cold stage and performing the droplet freezing experiment as described above. We note that on some occasions we observed unsatisfactory (i.e., there were freezing events at temperatures warmer than −15°C or more than half the droplets had frozen at temperatures warmer than −28°C) blank fraction frozen curves, which indicated that there was some contamination in the system (see section 3.1). Changing the water, cleaning the components of the system, and flushing the chamber with clean filtered nitrogen gas was sufficient to improve the background. We only ran an aircraft filter after two successful repeats of the blank experiments.

To check that the measured INP concentration per unit volume of air was independent of the volume of air sampled, as expected, the same air mass was sampled at different flow rates, simultaneously through both inlets. Each sample was collected over 30 min. To achieve this, during flight B929 (17 August 2015), a polycarbonate Nucleopore filter of pore size 0.2 μm was placed in the lowest level of one of the two filter holders, supported by a polythene mesh. The purpose of this filter was to restrict the flow, rather than for sampling. The air sampled through the unrestricted inlet, collected on filter B929_2, was thus ~2.5 times the volume as that simultaneously through the restricted inlet, collected on filter B929_1. Figure 5 shows the resulting INP concentration data for these two filters. Since a smaller volume of air flowed through B929_1, fewer aerosol particles were deposited and the probability of finding an INP at a given temperature was reduced. Hence, the freezing events observed on B929_1 were shifted to lower temperatures. In the region of overlap above around −20°C, the agreement is within 50%. This agreement shows that the flow rate made little difference to the INP concentration relative to other uncertainties.

2.4. Aerosol Size Distribution and Sampling Efficiency

Sampling of atmospheric aerosol in a representative way from an aircraft is a nontrivial task, and sampling problems, particularly with the coarse mode, have been documented for aircraft inlet systems, in general (Baumgardner & Huebert, 1993). Representative sampling of the coarse mode aerosol is particularly

problematic because these particles can be enhanced when sampling is subisokinetic (as is the case here), or they can be under-represented due to gravitational settling or inertial impaction on components of the inlet system. In the following we briefly review tests for sampling efficiency of coarse mode aerosol that have been performed with the inlet system we used in the present study.

Andreae et al. (2000) concluded that 35% of the coarse mode sea spray aerosol was collected on the filter. They made this estimate by comparing Na^+ concentrations from a filter sample collected by low flying aircraft (a few hundred meters sampled over about 30 min) to a sample collected from a ship in a similar location. Andreae et al. (2000) adjusted the bypass flow in order to maintain "slightly subisokinetic" sampling conditions. There are significant uncertainties with this estimate, and Andreae et al. (2000) suggest that the height difference alone could account for 20–30% of this difference since the sea spray loading at the surface will be larger than at a few hundred meters.

Young et al. (2016) compared size distributions determined from SEM analysis of filter-collected Arctic aerosol as part of the ACCACIA campaign with size distributions from under-wing probes. In these flights the filter sampling system on the FAAM BAe-146 aircraft was used in a very similar way to that in the present study. Young et al. (2016) kept the bypass fully closed and they used track etched polycarbonate filters. Hence, their samples were collected under similar subisokinetic conditions to those in this study. Under such conditions oversampling of coarse mode aerosol is expected. However, this was not observed by Young et al. (2016), whose results ranged from agreement within uncertainty between optical probes and SEM analysis, to far fewer coarse mode aerosol collected on the filter relative to the optical probes. The disagreement between 0.5 and 10 μm of these distributions implies that the inlet collection and filter efficiency issues were influencing these samples. They suggest that the discrepancy might also be a result of high RH, with the RH in the sampling periods being greater than 90%. Under such high RH conditions aerosol will be swollen with water, and therefore, the size distribution from the optical probes will be shifted to larger sizes compared to the SEM technique where samples are analyzed under dry conditions. In summary, the SEM technique, filter collection efficiency, and inlet losses could all be introducing some magnitude of error to the comparisons presented by Young et al. (2016).

In contrast to both Young et al. (2016) and Andreae et al. (2000), Chou et al. (2008) found that mineral dust coarse mode aerosol were oversampled on the filters. They based this on measurements of the size distribution using SEM and transmission electron microscopy and two Passive Cavity Aerosol Spectrometer Probes (PCASP), one mounted under a wing and one in the aircraft cabin. Chou et al. (2008) state that they adjusted the bypass flow in order to maintain "slightly" subisokinetic sampling conditions. It is not clear why Chou et al. (2008) oversample coarse mode aerosol while Andreae et al. (2000), who operated the system under similar conditions, undersampled coarse mode aerosol. A possible explanation is that many of the hygroscopic aerosol particles sampled by Andreae et al. (2000) were lost at the bend in the inlet pipework, whereas solid mineral dust aerosol may be more likely to bounce on impact at the bend and therefore find their way onto the filter.

In the present study, the average total aerosol surface area per unit volume of air corresponding to each filter sampling period was derived from particle size distributions measured by two open path underwing optical particle probes. The instruments were the PCASP and Cloud Droplet Probe (CDP). The PCASP measures particles with diameters in the approximate range 0.1–3 μm, and the CDP measures particles with diameters in the approximate range 2–50 μm. The derived size is affected by the optical properties of the particles (i.e., their complex refractive index) and their shape. Here the calibration method and optical properties correction method of Rosenberg et al. (2012) have been used. We use the value of 0.002 for the imaginary part of the refractive index (a value derived by Rosenberg et al. (2012) for African desert dust) to determine the surface area values that are presented in Table 1. This method uses Mie theory, which implies spherical particles. Despite the nonspherical nature of dust, Rosenberg et al. (2012) found this to be a good approximation for airborne dust. When calculating surface area, we again assume spherical particles for simplicity. A lognormal distribution function was fitted to each size distribution using a reduced chi-square method, and then the surface area and uncertainty in surface area were determined from the covariance matrix of these fits (the values are presented in Table 1).

In order to assess biases in sampling we have compared the size distribution of dust collected on 0.4 μm track etched polycarbonate filters with those determined from the under-wing probes (Figures 6 and 7). These

Table 1

Details of the 21 Successful Polytetrafluoroethylene Filters and the Two Scanning Electron Microscope-Analyzed Polycarbonate Filters (B926_1 and B931_1), Collected From the Facility for Airborne Atmospheric Measurements Aircraft During the Ice in Clouds Experiment-Dust Campaign

Flight	Filter number	Date	Start time (UTC)	End time (UTC)	Total sampled volume (standard liters)	Altitude (kft)	Aerosol surface area ($\mu m^2 \, cm^{-3}$)	Location	Temperature (K)	Dew point (K)
B920	2	7/8/2015	15:25:00	15:46:10	306	0.1	66.7 (6.4)	Northeast of Santiago	297.4 (0.3)	294.0 (1.0)
B920	4	7/8/2015	15:50:00	15:55:15	60	3.6	47.8 (8.2)	Northeast of Santiago	295.7 (0.6)	274.0 (7.2)
B920	6	7/8/2015	15:59:00	16:14:50	171	7.1	85.7 (8.8)	Northeast of Santiago	293.7 (1.6)	282.4 (2.4)
B921	2	10/8/2015	14:33:00	14:51:29	89	10.0	178 (20)	Northeast of Santiago	283.5 (0.1)	272.0 (0.8)
B921	4	10/8/2015	14:55:00	15:02:00	34	10.0	23.8 (7.4)	Northeast of Santiago	282.8 (0.2)	278.5 (0.4)
B921	6	10/8/2015	15:04:45	15:29:15	107	10.0	92.5 (9.7)	Northeast of Santiago	283.3 (0.5)	274.7 (3.6)
B922	2	11/8/2015	16:46:50	16:56:45	99	6.0	93.8 (10.9)	Southeast of Santiago	288.2 (0.4)	288.0 (0.7)
B924	4	12/8/2015	16:09:30	16:14:30	63	3.0	1318 (217)	Fuerteventura to Praia	301.4 (0.4)	284.3 (0.7)
B924	6	12/8/2015	16:17:40	16:22:40	62	3.0	1673 (228)	Fuerteventura to Praia	302.0 (0.3)	285.5 (0.3)
B924	8	12/8/2015	16:25:25	16:29:25	50	3.0	1874 (220)	Fuerteventura to Praia	299.3 (0.2)	286.3 (0.3)
B925	2	13/8/2015	15:03:10	15:28:10	111	10.0	175 (16)	South of Santiago	283.0 (0.2)	272.9 (1.4)
B926	1	14/8/2015	15:29:50	16:24:00	1167	7.5–8.0[a]	133 (14)	Southeest of Praia	287.3 (0.4)	281.4 (1.0)
B926	2	14/8/2015	15:29:50	16:24:00	430	7.5–8.0[a]	133 (14)	Southwest of Praia	287.3 (0.4)	281.4 (1.0)
B927	2	15/8/2015	16:21:30	16:42:20	134	8.0[b]	628 (63)	North of Santiago	287.1 (0.7)	282.5 (0.9)
B928	2	16/8/2015	15:13:18	15:38:00	397	0.1	204 (23)	West of Santiago	299.7 (0.3)	297.9 (0.9)
B928	4	16/8/2015	16:01:50	16:23:42	132	9.0	212 (19)	West of Santiago	286.1 (0.1)	276.6 (0.4)
B928	6	16/8/2015	16:55:10	17:18:08	89	10.8	688 (128)	West of Santiago	281.8 (0.2)	277.8 (1.1)
B929	1	17/8/2015	16:06:55	16:36:53	98	8.0	511 (53)	South of Santiago	286.0 (0.3)	282.0 (0.5)
B929	2	17/8/2015	16:06:55	16:36:53	248	8.0	511 (53)	South of Santiago	286.0 (0.3)	282.0 (0.5)
B931	1	19/8/2015	16:42:03	16:51:21	377	0.1	97.6 (8.4)	South of Santiago	300.2 (0.3)	296.1 (1.7)
B931	2	19/8/2015	16:42:03	16:51:21	108	0.1	97.6 (8.4)	South of Santiago	300.2 (0.3)	296.1 (1.7)
B932	2	20/8/2015	11:01:47	11:17:00	156	0.1	132 (17)	West Coast of Africa	297.1 (0.1)	295.0 (0.9)
B932	6	20/8/2015	11:48:09	12:03:09	95	11.5	419 (46)	West Coast of Africa	280.6 (0.2)	272.1 (1.4)

Note. The surface area was derived from the Cloud Droplet Probe and Passive Cavity Aerosol Spectrometer Probes measurements, and the numbers in brackets in the aerosol surface area column are the uncertainty in that derived data. The temperature is the mean true air temperature measured by the non-de-iced Rosemount temperature probe, and the dew point is recorded by the Buck CR2 chilled mirror hygrometer. The numbers in brackets after the temperature and dew point are the standard deviations in the recorded data across the run for which each filter was sampled (this does not represent the overall uncertainty in these measurements).
[a]Altitude was varied during collection to stay within dust layer. [b]Filter was exposed during descent to 8.0 kft (altitude was constant at 8.0 kft from 16:23:30 onward).
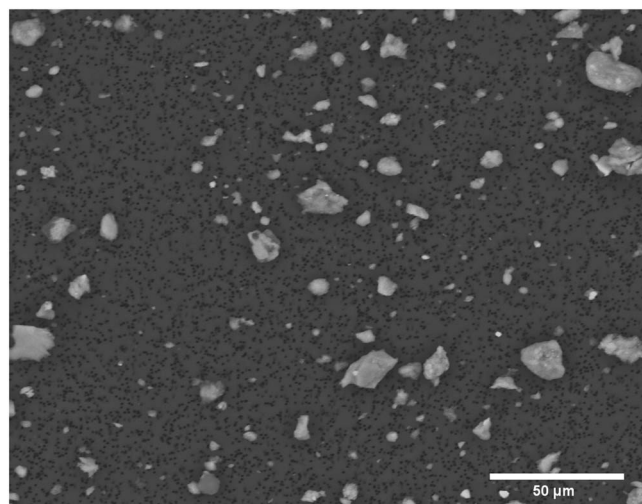

Figure 6. Scanning electron microscope image of aerosol particles sampled on a track etched polycarbonate filter during flight B926. The dark circular shapes in the background are the 0.4 μm pores in the filter, while the particles are lighter in color. The scale bar is 50 μm.

filters were collected in parallel with the Teflon filters we used for the INP analysis for a subset of the filter runs and then analyzed using SEM. The analysis is set out in detail by Young et al. (2016). Examples of SEM size distribution compared to the CDP/PCASP distribution, and an SEM image (Figure 6), are shown in Figure 7. These results indicate that there is enhancement of the coarse mode aerosol particles on the filters relative to the underwing probe size distributions, a similar result to Chou et al. (2008). This is consistent with oversampling of coarse mode aerosol due to the subisokinetic sampling conditions. The integrated surface areas were within a factor of 2.5 between the SEM and optical probes (see caption of Figure 7). This discrepancy should be borne in mind when interpreting the INP data presented later in the paper, which are not corrected for sampling biases, since the sampling biases themselves are uncertain. It should also be noted that the flow rate through the polycarbonate filters for SEM analysis was greater than for the Teflon filters for INP analysis (by a factor of 2.7 and 3.4, for filter pairs from B926 and B931, respectively). Hence, there may be differences between the sampling efficiency between the two filters. However, we do have filter samples for INP analysis sampled in parallel, but with different flow rates. (Figure 5, see discussion above). There the flow rate differed by a factor of 2.5, but there is good agreement between the INP concentrations
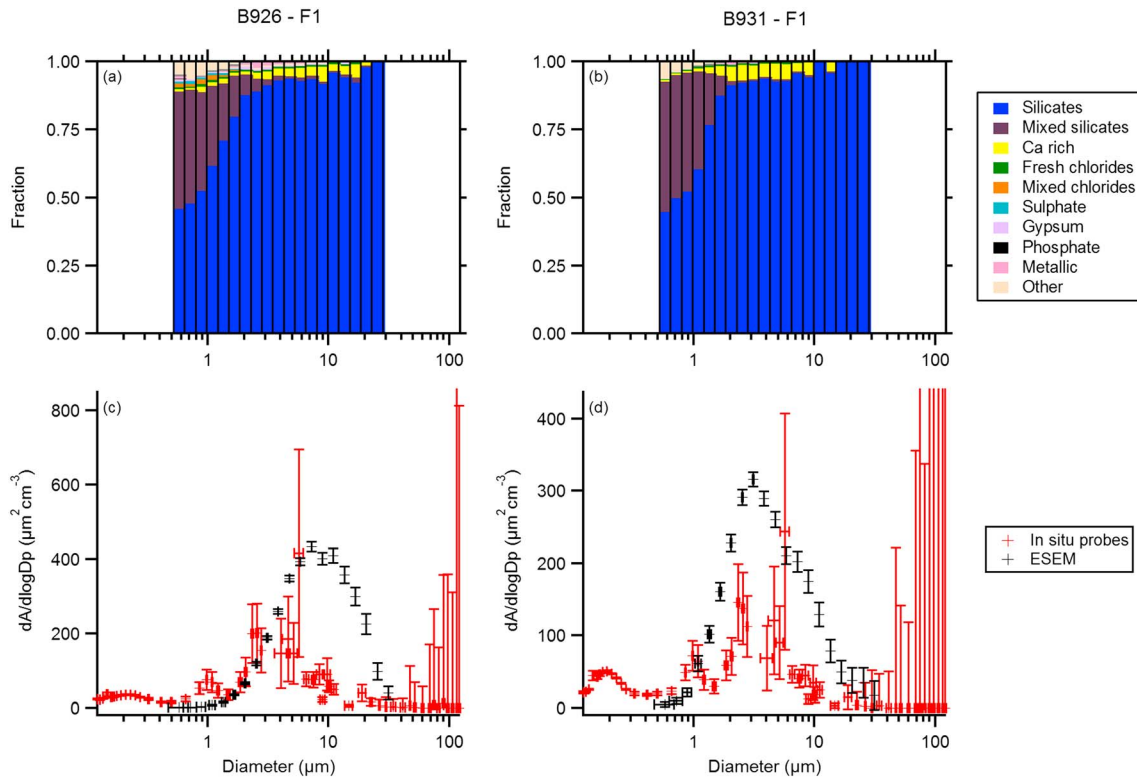
Figure 7. The size resolved composition and size distribution of samples collected in dusty air (B926: 133 ± 14 μm^2 cm^{-3}; B931: 98 ± 8 μm^2 cm^{-3}). Filter B926_1 was from 7.5 to 8 kft, and filter B931_1 was sampled at 100 ft; hence, the two filters represent very different sampling conditions. The flow rate was 21 sLmin^{-1} and 40 sLmin^{-1} for filters B926_1 and B931_1, respectively. The in situ size distribution was determined from the PCASP and CDP optical probes and is compared with a distribution determined by SEM. The surface area determined from the SEM analysis was 338.9 μm^2 cm^{-3} (B926) and 245 μm^2 cm^{-3} (B931). For these filter samples, the surface areas are within a factor of 2.5 of the surface areas determined from the underwing in situ probes.
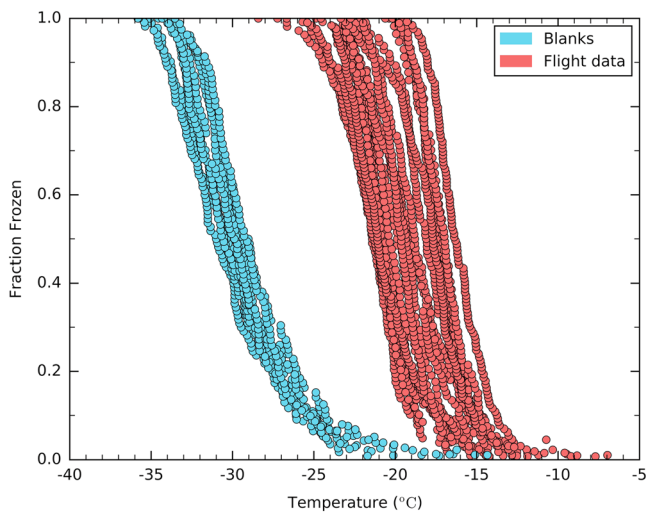

Figure 8. Fraction frozen curves for drop freeze assays performed during the Ice in Clouds Experiment-Dust campaign in August 2015. Aircraft samples are shown in red, while blanks with pure water droplets directly on clean filters are shown in blue.

determined from the two filters, indicating that sampling is not sensitive to flow conditions under these specific conditions.

3. Results and Discussion

3.1. INP Concentration Measurements

Details of 21 filter samples collected for INP analysis during the ICE-D campaign are given in Table 1, and Figure 8 shows the corresponding fraction frozen curves from the drop freeze assays. Also shown, in light blue, are the fraction frozen curves recorded when the shiny side of clean filters was tested in the temporary laboratory in Cape Verde. It can be seen that there is a clear difference in ice nucleation temperatures between the blank and the exposed filters.

The data in Figure 8 are used to determine the temperature-dependent INP concentration for each filter sample. These are shown in Figure 9a. The measured INP concentrations span more than 3 orders of magnitude between 10^2 to 10^5 m^{-3}, over temperatures ranging from about -10 to $-25°C$. The range of INP concentrations the technique is sensitive to is determined by factors such as sampling volume, aerosol loading, and droplet size. There is also significant variability in the INP concentration at a given activation temperature; for example, at $-20°C$ the INP concentration ranges from about 10^3 m^{-3} to 10^5 m^{-3}.
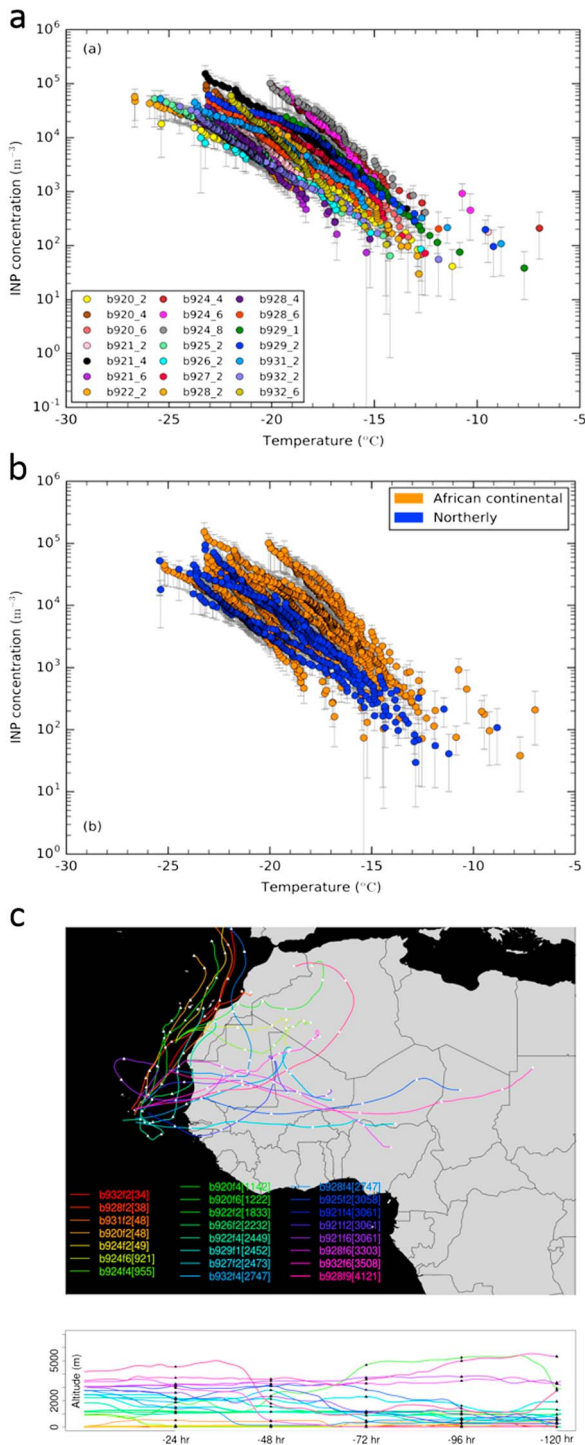
Figure 9. Measured ice-nucleating particle concentration ([INP](*T*)) for all filter measurements during Ice in Clouds Experiment-Dust. (a) All the filter measurements are shown and are color coded. (b) The measurements are grouped using back trajectory analysis into air masses dominantly originating in Africa and air masses originating from the North of Cape Verde, possibly with marine influence. (c) The back trajectories are summarized where the color corresponds with height (the height corresponding to each filter sample is given in brackets in the key, in meters). Low-level (<100 m) flights sampled air dominantly from the North of Cape Verde, which may have had some marine, European and African influence. Filter samples collected at higher altitudes tended to come from North Africa.

In Figure 9b the results from the individual filter runs are divided into two categories according to a back trajectory analysis. A summary of the Hybrid Single-Particle Lagrangian Integrated Trajectory (HYSPLIT) back trajectory analysis (Stein et al., 2015) is given in Figure 9c. The starting points for the trajectories were the averaged values of the latitude, longitude, and height of each filter run. HYSPLIT back trajectories are based on large-scale meteorological data, which do not represent convection or turbulence. However, most of the convective cloud systems in this study were to the south; hence, the flow patterns were generally not complicated by convection. In order to test the sensitivity to starting point, we used the ensemble mode where multiple trajectories are run with variable starting locations; the trajectory in Figure 9c is for the principle trajectory, which is generally representative of the ensemble. In general, filter samples taken at low altitude tended to sample air that had traveled from the north of the Cape Verde islands with the air masses sometimes skirting the coast of Africa (labeled "Northerly" in Figure 9b). Most of the other trajectories indicate sampled air, which traveled over continental North Africa (labeled "African continental" in Figure 9b). We left data from several filter samples out of Figure 9b (B922_2, B925_2, and B926_2) because they had more complicated trajectories and did not clearly fit into these two categories. The air from both trajectories was dust laden, but the concentration of dust in the African continental samples was much more variable and could be much larger than in the Northerly group. There is a 2 order of magnitude variability in the INP concentration of the samples with African continental trajectories, whereas those with a Northerly trajectory are more uniform and generally at the lower end of, but overlapping with, the African continental range. The highest INP concentrations in the African continental category correspond to the flight with the highest aerosol loadings when we flew through an optically thick dust layer (B924). It should be noted as well that this flight sampled aerosol much closer to its source region.

In Figure 10 we compare our INP concentrations (all measurements shown in Figure 9b) with the INP concentrations predicted by the parameterization of DeMott, Prenni, et al. (2015) for INP concentrations in dusty air (referred to as D15 from hereon). This parameterization uses the concentration of aerosol particles larger than 0.5 μm (from the optical probes) and activation temperature to determine INP concentration. The parameterization is empirically based upon laboratory studies, conducted below −19°C, of desert dust samples using a continuous flow diffusion chamber (CFDC) as well as a cloud expansion chamber. D15 also show that their parameterization is consistent with aircraft observations in dusty air over the Caribbean. The data from our study and the D15 parameterization agree to within about 1 order of magnitude. However, there are differences between the two general categories defined by back trajectories (African continental and Northerly, defined above). The D15 parameterization tends to predict INP concentrations up to an order of magnitude higher than our measurements for the African continental group, with a greater difference at smaller INP concentrations, which correspond to higher temperatures. The largest discrepancies are for higher temperatures and lower INP concentrations, where the D15 parameterization is extrapolated beyond the range of temperatures (> −19°C) of the measurements
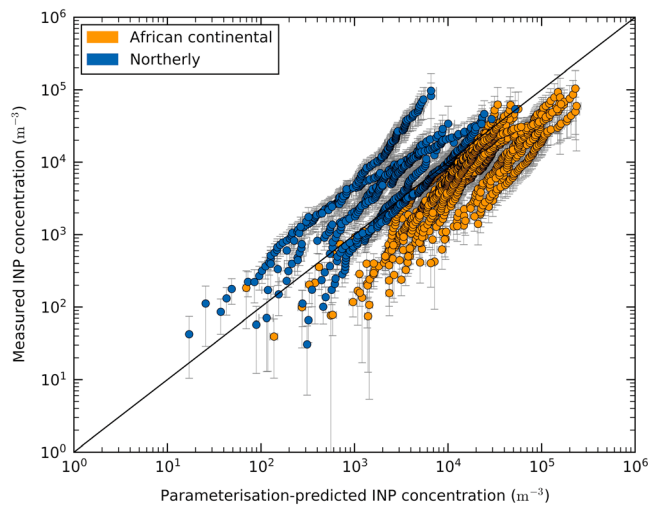
Figure 10. Comparison of the measured ice-nucleating particle concentrations with those predicted by the parameterization of DeMott, Prenni, et al. (2015) for data set split into the two categories defined in Figure 9. This parameterization is specifically for dust-laden air and relates the ice-nucleating particle concentration to the concentration of particles larger than 0.5 μm and temperature. We apply a factor of 3 correction factor recommended by the authors. We removed two runs from this plot where the uncertainty in a small concentration of aerosol larger than 0.5 μm was very large. The concentration of particles larger than 0.5 μm is taken from the optical probe size distributions (e.g., Figure 7); the uncertainty associated with this quantity is shown, but typically of a similar size to the data points.

on which it was based. This greater difference at higher temperatures is illustrated in Figure 11a for a high dust loading case (B924). In contrast, the D15 parameterization tends to predict lower values, by up to an order of magnitude, than measured INP concentrations for the Northerly group. In general, the Northerly group (Figure 9) may have had some marine influence, and therefore, some fraction of the coarse mode aerosol may have been sea spray aerosol. However, the presence of a significant component of coarse mode aerosol such as sea spray, which is less active than desert dust for a similar size particle, would tend to lead to an overestimate in the D15 INP concentration rather than an underestimate. Also, the SEM analysis in Figure 7 for a Northerly run sampled at an altitude of only 100 ft (30.5 m) shows that the particles on this filter were dominated by mineral dust, with very little detectable sea salt. Some of the Northerly trajectories originated close to Europe and passed by the North African coast and may have been influenced by more active aerosol types such as biological materials had a different dust mineralogy or perhaps contained small (<500 nm) sea spray aerosol, which was too small to be detected using the SEM technique.

3.2. High Dust Loading Case Study

We sampled in an optically thick dust layer at ~3 kft (~915 m), which was situated between Cape Verde and the Canary Islands on 12 August 2015 (flight B924). This was a very dense dust layer with aerosol number concentrations in the coarse mode of ~200 cm^{-3} and aerosol surface areas of ~1,500 $\mu m^2\ cm^{-3}$. The resulting INP data are shown in Figure 11a. Due to the high dust loading, a short sampling time of 5 min was used, which allowed us to take three consecutive filter samples in quick succession in the same layer. The INP concentrations determined from these three filter samples, shown in Figure 11a, are within measurement uncertainty of each other indicating that along the flight track the dust layer was relatively uniform in its ice-nucleating ability.

The approximate origin of the dust plume we sampled on 12 August can be deduced from Meteosat Second Generation Spinning Enhanced Visible and InfraRed Imager images. In Figure 11b we show a sequence of images where dust is shown in pink (not to be confused with deep red color for clouds). On 9 August a dust signal appears on the border between Niger and Algeria (circled). This dust feature intensifies by 10 August and moves to the north and west in a manner consistent with a haboob, which is generated by strong winds associated with the outflow from organized deep convection (Knippertz & Todd, 2012). By 11 August the dust plume spreads out and on 12 August at 11:00 UTC, 5 h before we took the filter samples corresponding to the data in Figure 11a, part of the dust plume has moved out over the Atlantic south of the Canary Islands. Hence, on this occasion, we can correlate the intense dust plume we sampled on 12 August with a dust emission event on 9 and 10 August. Prospero et al. (2002) note that there are well-defined dust sources in an area bounded by the Ahaggar mountains to the north in Algeria, the Massif de l'Air to the south east, and the Adrar des Ifoghas in Mali to the west. Based on satellite data, Prospero et al. (2002) also note that the most persistent source in this region is associated with a large system of ephemeral water courses that drain the Massif de l'Air. In the soil mineralogy maps of Nickovic et al. (2012) this region is characterized by desert soils with 10–20 wt % by mass of feldspar (all feldspars including K-feldspar), as well as quartz, clays, and other minerals. Hence, this region is likely a source for ice-active feldspar dusts. Overall, this case study of an individual dust plume illustrates that that it is possible to trace particular events back to emission in particular regions and associate them with particular meteorological events. In principle, this could be done systematically in the future and the ice-nucleating activity associated with each event correlated with emission factors, such as location, types of dust emitted (e.g., mineralogy, ephemeral rivers, and lakes), and meteorological events associated with the dust emission.

3.3. Ice Active Site Density for Desert Dust Dominated Aerosol

Many of the filter samples were taken in very dusty conditions where the aerosol composition, and therefore surface area, was dominated by silicates, which comprise a large fraction of desert dust (this can be seen in
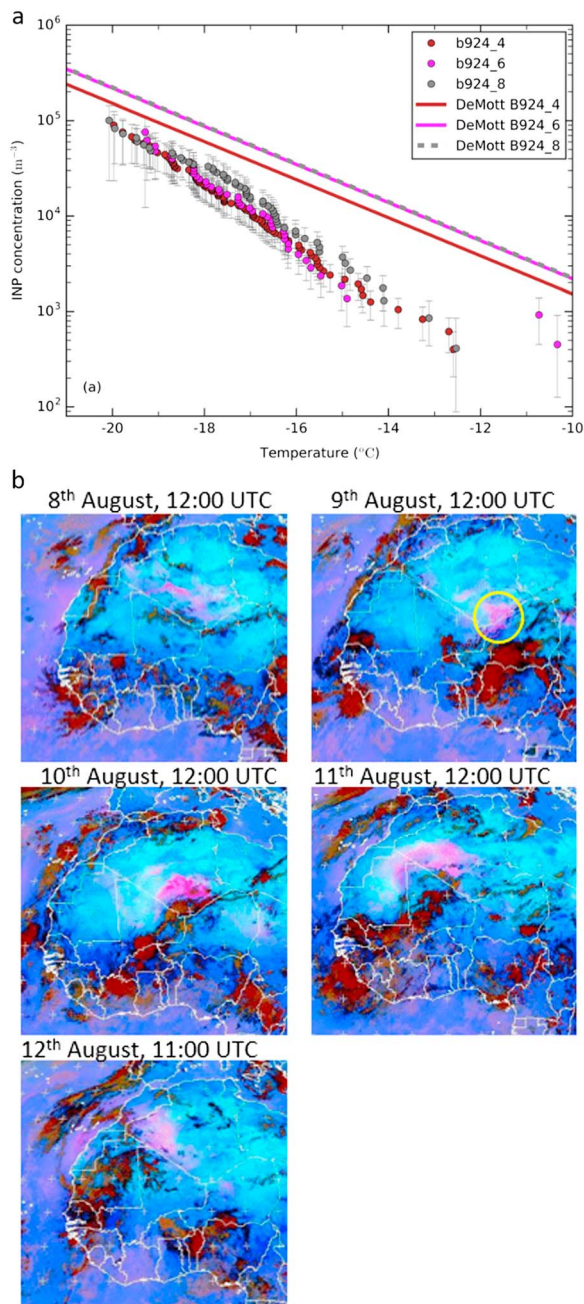
Figure 11. Ice-nucleating particle measurements from flight B924 on 12 August 2015 in an optically thick dust layer between the Canary Islands and Cape Verde. The three samples collected were collected in quick succession at the same altitude. (a) The ice-nucleating particle concentrations were very similar in each filter sample. We compare our results to the parameterization of DeMott, Prenni, et al. (2015); note that this parameterization is based on data below −19°C. (b) Meteosat satellite images where pink colors indicate dust aerosol and dark red indicates clouds. We present images from 8 to 12 August, the day which corresponds to the measurements in Figure 11a. A strong dust signal emerges on 9 August in the region of the border between Niger and Algeria (circled). On subsequent days this dust plume intensifies and moves north and west until it spreads out over the Atlantic south of the Canary Islands. The last image was for 11:00 UTC, and our filter sampling was some 5 h later. We acknowledge EUMETSAT for the Meteosat Second Generation Spinning Enhanced Visible and InfraRed Imager images.

the SEM analysis presented in Figure 7). This presents an opportunity to determine the temperature-dependent cumulative density of active sites, n_s for aerosol, which is dominantly desert dust. We refrain from referring to this material as mineral dust because the particles of air-borne desert dust may also contain salts and possibly biological residues from the desert source region, which may be important for ice nucleation. This material has also been in the atmosphere for several days so may have been aged to some extent by interaction with other atmospheric constituents. The composition analysis shown in Figure 7 identifies the major component(s) of individual particles but is limited in its ability to identify mixtures of different particle types. Once air-borne, desert dust also has the potential to be influenced by atmospheric gases and mix with other aerosol types. These processes may influence the ice-nucleating ability of transported desert dust. Hence, comparison of laboratory-based parameterizations for desert dust with n_s for desert dust dominated aerosol relatively close to source regions will help inform how representative the laboratory-based parameterizations are for desert dust dominated aerosol in the atmosphere.

In order to compare to literature parameterizations for desert dust we have taken a subset of high aerosol loading filter samples (>100 μm^2 cm^{-3}) and derived n_s for this subset. The choice of this threshold was informed by the SEM analysis where it is clear that the coarse mode is dominated by mineral dust aerosol (see Figure 7). We define n_s for desert dust dominated aerosol as (Connolly et al., 2009; DeMott, 1995):

$$n_s = [INP]/A_{aer} \qquad (3)$$

where A_{aer} is the total surface area of the aerosol per unit volume of atmosphere derived from the underwing optical probes (see methods section). It must be noted that we observe an enhancement of coarse mode aerosol on the filters, as discussed earlier, which means our derived n_s is likely to be biased high. This is discussed in more detail below.

The subset of n_s for desert dust dominated aerosol is shown in Figure 12, where each point corresponds to a droplet freezing. The data in Figure 12 are from filter samples, which were collected at altitudes from 100 to 11,500 ft (30.5 to 3,350 m), and the back trajectories suggest variable air mass histories (as illustrated by the back trajectory analysis in Figure 9). Despite the variability in air mass histories, the variability in n_s at a given temperature for these samples is only about 1 order of magnitude. The suggested relatively minor dependence on dust source region is consistent with the similar conclusions from previous studies of ice nucleation by desert dusts (DeMott, Prenni, et al., 2015; Kaufmann et al., 2016; Niemand et al., 2012).

In addition to our data, in Figure 12, we plot n_s determined using a CFDC situated within the Saharan dust layer at a mountain-based observatory in the Canary Islands (Boose, Sierau, et al., 2016). We only plot data corresponding to 103% RH in what Boose, Sierau, et al. (2016) classify as strong dust events. The two data sets agree to within an order of magnitude in the temperature regime in which they overlap (at −25°C), despite being obtained with very different instruments. However, it should be noted that Boose, Sierau, et al. (2016) did not apply a factor to account for the potential insufficient droplet
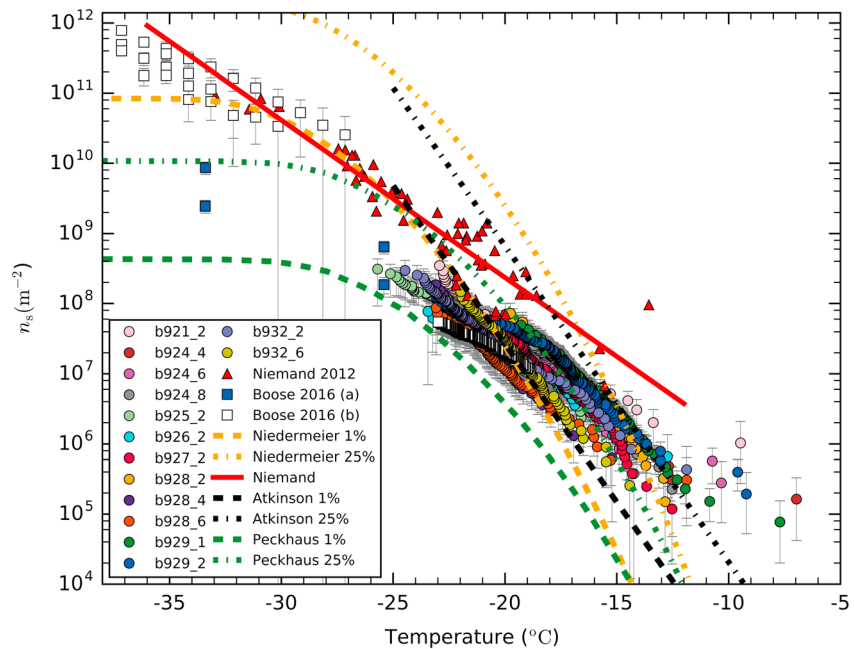
Figure 12. Values of n_s for desert dust dominated aerosol compared to a range of laboratory based parameterizations and data as well as other literature measurements of n_s for desert dust dominated aerosol. In this plot, we only include filter samples where the aerosol surface area was larger than 100 μm^2 cm^{-3}, i.e., where the coarse mode is most likely dominated by desert dust (see text for discussion). We compare these data sets to an n_s parameterization for desert dust (Niemand et al., 2012) and several scaled K-feldspar parameterizations (Atkinson et al., 2013; Niedermeier et al., 2015; Peckhaus et al., 2016). In addition, we compare our results to the n_s derived for aerosol in a dust event in the Canary Islands (Boose, Sierau, et al., 2016) as well as laboratory measurements of desert dust sampled from the air or by sampling dust, which has deposited on the ground (Boose, Welti, et al., 2016).

activation in their CFDC instrument. DeMott, Prenni, et al. (2015) corrected (enhanced) their CFDC INP concentrations by a factor of 3. A similar enhancement to the data of Boose, Sierau, et al. (2016) would result in n_s values, which are still in reasonable agreement with our values.

We also compare our n_s for desert dust dominated aerosol with several laboratory data sets. We plot the parameterization of desert dust n_s from the AIDA cloud expansion chamber (Niemand et al., 2012) (referred to as N12 from hereon). This parameterization is valid between −12 and −36°C where the bulk of the measurements was made below −19°C (the data points from N12 have also been included in Figure 12). A revised parameterization has very recently been produced with new data from the AIDA chamber for desert dusts (Ullrich et al., 2017), and the resulting parameterization is very similar to N12. The values of n_s from the N12 parameterization are larger than the n_s values for our desert dust dominated aerosol samples. Boose, Welti, et al. (2016) report laboratory measurements of ice nucleation by desert dust samples, which were collected from the air or by sampling dust that had deposited on surfaces (they also show results for sieved and ground desert dust samples, but these are not as relevant as the dust samples that had undergone transport through the air and they are omitted for simplicity). Two separate sets of experiments are reported by Boose, Welti, et al. (2016), one with a CFDC fitted with a chamber designed to activate aerosol to droplets prior to aerosol entering the CFDC (IMCA-ZINC) and one with the Frankfurt Ice Deposition Freezing Experiment (FRIDGE) operated in the freezing mode. The IMCA-ZINC results are in good agreement with the N12 parameterization, whereas the FRIDGE measurements are in good agreement with the results of the present study.

There are a number of possible explanations for the discrepancies between our results and the desert dust parameterization of Niemand et al. (2012). An obvious issue with the aircraft sampled particles examined in this study is that there are sampling biases (these are discussed in section 2). However, the comparison of the SEM with in situ optical probes (Figure 7) suggests that there may be an enhancement of coarse mode particles on the filters, which indicates that the surface area we use to derive n_s is too small by a factor of

around 2.5 (at least for the two filters we analyzed with SEM). The oversampling is a product of both oversampling of the coarse mode at the inlet and also losses of aerosol in the pipework. But, the implication of oversampling is that our reported n_s values may be biased high, which suggests an even greater discrepancy between our results and those of Niemand et al. (2012). Discrepancies between various instruments have been observed for the ice-nucleating ability of a mineral dust during an instrument intercomparison (Hiranuma et al., 2015). The average n_s from instruments for nx-illite with dry dispersed particles was larger than those with wet-dispersed particles. However, several CFDC instruments (dry dispersed) reported n_s values consistent with cold stage droplet freezing instruments (wet-dispersed), which are inconsistent with a simple dry-versus-wet discrepancy. Furthermore, the FRIDGE instrument (in immersion mode) produced n_s values up to about 2 orders of magnitude larger than many other droplet freezing instruments for nx-illite, whereas the agreement between FRIDGE data and our data in Figure 12 is very good. Nevertheless, when interpreting the data in Figure 12, it should be borne in mind that there are documented and unexplained discrepancies between different instruments. Alternatively to an instrumentation or sampling issue, it could be argued that in the desert dust dominated aerosol that we (and Boose, Sierau, et al. (2016)) sampled, only around 10% of the surface area was desert dust and the remaining surface area was made up of less ice-active aerosol. However, this seems very unlikely given that the SEM/EDX analysis indicates that the aerosol composition was dominated by mineral dust particles. The explanation for this discrepancy may also be that there is a difference between airborne desert dust and desert dust collected from the surface and then aerosolized for chamber experiments. For example, the dust samples taken from the surface and aerosolized in the laboratory and those aerosolized through wind-driven processes may differ in their ice-nucleating ability. In addition, in the atmosphere desert dust mixes with other chemical species, including acids. It is well known that acids can deactivate desert dust (Augustin-Bauditz et al., 2014), and it is possible that the desert dust dominated aerosol we sampled here had suffered some degradation in its ice-nucleating ability due to aging processes.

We also compare K-feldspar n_s parameterizations from Atkinson et al. (2013), Niedermeier et al. (2015), and Peckhaus et al. (2016) (referred to as A13, N15, and P16, respectively) in Figure 12. K-feldspar is thought to be the most ice-active mineral in desert dust and typically makes up between 1 and 25% of airborne desert dust mass (Atkinson et al., 2013); hence, we scale the K-feldspar n_s parameterizations to 1 and 25% making the assumption that K-feldspar also makes up this fraction of the dust surface area. This rough approximation has been used in the past to estimate the ice-nucleating ability of agricultural and desert soils (Atkinson et al., 2013; O'Sullivan et al., 2014). The A13 parameterization for K-feldspar (black dotted-dash line) is a good match to the slope and magnitude of n_s for most of the filter measurements above ~ −19°C, but overpredicts the activity at lower temperatures. A minority of the data points sit above the A13 line above −12°C, but these data points make up only ~0.5% of the data points included in the plot and the uncertainty of these "sporadic" points tends to be relatively high. The N15 parameterization (orange dotted-dash line) also tends to overpredict relative to the new data for our samples of desert dust dominated aerosol. The P16 parameterization (green dashed line) is a good predictor of n_s values for both our measurements and those of Boose, Sierau, et al. (2016) below about −19°C, but underpredicts our n_s at higher temperatures. While none of the available literature parameterizations fit the n_s values for desert dust dominated aerosol across the entire temperature range, it should be noted that the new data are consistent with the various parameterizations within about 1 to 2 orders of magnitude. Hence, the laboratory-derived parameterizations for desert dust go some way to providing an approximation for the n_s values we measure for our aircraft-collected samples of desert dust dominated aerosol.

3.4. Comparison of the Measured INP Concentrations With the Predictions of a Global Aerosol Model

In Figure 13 we plot the modeled INP spectra for K-feldspar from desert sources and marine organics associated with sea spray, where the range in values represent the range in model daily means during August. For these model predictions, we have used the Global Model of Aerosol Processes for the grid box corresponding to Cape Verde (2.8 by 2.8°). The version of this model from which the data have been extracted is described in detail by Vergara-Temprado et al. (2017). The model is based on the year 2001 meteorology. The K-feldspar INP spectrum is from the A13 parameterization, and the K-feldspar distribution in the model is predicted based on wind speed-dependent desert dust emission together with the regionally resolved dust mineralogy from Nickovic et al. (2012). The marine organics INP spectrum is based on measurements of the
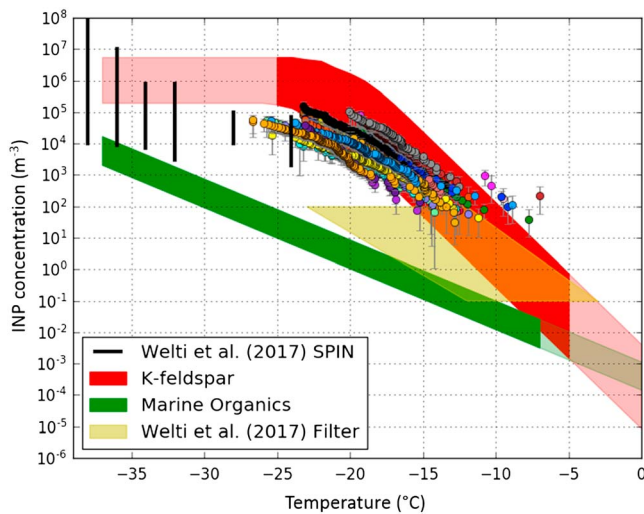
Figure 13. Ice-nucleating particle concentration as a function of activation temperature for marine organic aerosol and K-feldspar from the Global Model of Aerosol Processes (GLOMAP-mode) (Vergara-Temprado et al., 2017). The lighter shaded regions of the two curves indicate where the parameterizations are extrapolated. Model output is shown for the grid box around Cape Verde and represents concentrations for August (based on meteorology from the year 2001) for altitudes up to 11,500 ft. The breadth of the model lines indicates the model variability in the daily means during the month of August. In addition to comparing the model output with data from the present study (from Figure 9), we also compare to recent data from a ground-based station in Cape Verde (Welti et al., 2017).

INP content per organic mass of ocean microlayer samples (Wilson et al., 2015). This is consistent with DeMott, Hill, et al. (2015) who found that the INP concentrations from artificial sea spray are consistent with measurements of aerosolized INP in a wave tank and in the remote marine atmosphere. The width of the lines for K-feldspar and marine organic INP represent the variability in the daily means. These span relatively low dust loading days to days influenced by strong dust events. In the tropical Atlantic near Cape Verde, the model predicts that desert dust is more important than marine organics in the entire temperature range over which our measurements were made.

We have also overlaid all INP concentration measurements made during the present study, which represent a range of conditions from dust outbreaks to more quiescent situations (Figure 13). Comparison of field measurements to a global model output raises the question of representivity. In this case we think this is justified on the basis that a relatively large number of filter samples were acquired over a relatively large spatial scale in a range of conditions. Above ~ −20°C the agreement between the field measurements and the model in both the magnitude and variability in INP concentrations is very good. At lower temperatures, the model tends to overpredict the INP concentration of these samples, which is consistent with Figure 12 where the A13 parameterization overpredicts n_s relative to our determination of n_s for airborne samples. In addition, a high bias at low temperatures in the modeled INP concentrations has been noted at other locations around the world (Vergara-Temprado et al., 2017). Nevertheless, overall, the model reproduces the measured INP concentrations reasonably well.

3.5. Implications for the Hallett-Mossop Ice Multiplication Process in Tropical Atlantic Convective Clouds

Convective clouds that form in the eastern tropical Atlantic have the potential to form clusters, which can develop into tropical storms or hurricanes and were a major focus for the ICE-D campaign. Convective clouds are commonly thought to be impacted by secondary ice production mechanisms such as the Hallett-Mossop process where the freezing of a small number of large droplets and subsequent riming are thought to produce copious quantities of ice splinters (Field et al., 2017). Thus, the ice concentration in these clouds can greatly exceed the INP concentration (Crawford et al., 2012; Rangno & Hobbs, 2005). The Hallett-Mossop process is thought to peak in efficiency at a temperature of around −5°C, and be active between around −3 and −8°C (Pruppacher & Klett, 1997). It is not clear what concentration of INPs is needed in order to trigger the Hallett-Mossop process, but it has been estimated that only 0.01 to 10 m^{-3} are required (Beard, 1992; Crawford et al., 2012). Recently, Huang et al. (2017) concluded that 10 m^{-3} is sufficient to trigger the Hallett-Mossop process provided that the other criteria for this process are met (including sufficient numbers of large and small droplets in the correct temperature range), but a reduction to 1 m^{-3} in the primary ice concentration inhibits its effective operation. Hence, the concentration and identity of INPs in the Hallett-Mossop regime are of primary interest.

The bulk of the INP data from the present study does not cover the Hallett-Mossop temperature regime, but we can derive limiting values and also use our global aerosol model to predict the INP concentration at higher activation temperatures. The INP data from this work define an upper limit of the INP concentration of approximately 100 m^{-3} (i.e., approximately the lowest values in our data set); i.e., the INP concentration in the Hallett-Mossop regime is not more than about 100 m^{-3}. This is consistent with the measurements presented by Welti et al. (2017), who made measurements of INP from the Cape Verde atmospheric observatory over a period of 4 years (also shown in Figure 13). The bulk of their measurements are made with a filter-based technique, which is sensitive to concentrations as low as 0.1 m^{-3}, but they also used a thermal gradient diffusion chamber (CFDC) for a limited period of time for measurements at higher INP concentrations at lower temperatures. The CFDC measurements are in good agreement with our measurements where they overlap

at -25°C. Their filter-based results extend over a broader range of INP concentration than our global model predicts for K-feldspar INP and our INP measurements, but the upper limit to their measurements is in good agreement with our model predictions. There have been suggestions that biogenic INP might be important in dusts from arid regions (Schnell, 1974a; O'Sullivan et al. 2016), but these results indicate that in this location this is not the case. Overall, the model and field data suggest that INP concentrations from K-feldspar are only 10^{-3} to 1 m^{-3} at -5°C. It is not completely clear whether this is enough to trigger sufficient primary ice production to allow secondary ice production to become active; however, several of the papers cited above suggest that these low concentrations may be sufficient.

4. Conclusions

A filter and cold-stage method is described to measure the concentration of immersion-mode INPs collected from an airborne platform. The method was used successfully to quantify the INP spectra in the tropical Atlantic during August 2015. We present the INP concentrations over a range of altitudes from 100 ft (30.5 m) through to 11,500 ft (3.5 km), sampling air with a wide range of aerosol loadings. The highest INP concentrations, up to 10^5 m^{-3} at -20°C, were measured on 12 August in an optically thick dust layer where the aerosol surface area was 1,300–1,900 μm^2 cm^{-3} with a particle concentration of ~200 cm^{-3} ($>$0.5 μm). In contrast, the lowest INP concentrations, ~10^3 m^{-3} at -20°C, were measured when the aerosol concentration was less than 10 cm^{-3} ($>$0.5 μm).

When the INP concentrations were normalized to aerosol surface area in dust laden air, active site densities were produced, which agreed with one another within about an order of magnitude. Our results are also consistent with the only other measurements of n_s for desert dust dominated aerosol close to the North African continent, which were made using a CFDC from a mountain top observatory in the Canary Islands (Boose, Sierau, et al., 2016). We compared the ice active site densities determined from our data to those of a range of laboratory-based parameterizations and measurements in order to test how well these can represent the ice-nucleating ability of a desert dust dominated aerosol. There are numerous processes that could lead to airborne desert dust aerosol having different ice-nucleating ability to idealized proxies used in the laboratory. These include acid processing or mixing with other aerosol types. We conclude that within 1 to 2 orders of magnitude, depending on temperature, the laboratory-based parameterizations for desert dust have some skill in predicting the ice nucleation ability of desert dust dominated aerosol.

In the past it has been suggested that that the ice-nucleating ability of desert dusts from different deserts around the world have a relatively uniform ice-nucleating ability (Boose, Welti, et al., 2016; Kaufmann et al., 2016; Niemand et al., 2012). Our study is consistent with this suggestion since the back trajectories indicated that the dust sources were from across a wide area of North Africa. This could indicate that a particular ubiquitous component of desert dust is responsible for its ice-nucleating ability. In the past it was suggested that this component is K-feldspar and this is supported by the present study where it was shown that the airborne sampled n_s values are consistent with the typical feldspar content of desert dust. However, there are discrepancies between the different K-feldspar parameterizations (Atkinson et al., 2013; Niedermeier et al., 2015; Peckhaus et al., 2016), with no single K-feldspar parameterization providing a predictive capacity over the whole temperature range.

While our measurements of INP concentrations in the eastern Atlantic are the first in this region made from an aircraft, they are limited in the temperature and INP concentration range over which they extend. Ideally, we would be able to make measurements within the temperature regime relevant for the Hallett-Mossop ice multiplication regime at around -5°C. While our measurements place an upper limit of 100 m^{-3} of INP above -10°C, our model predictions suggest an INP concentration of 10^{-3} to 1 m^{-3} for feldspar. It is not clear whether this small concentration of feldspar INP could trigger secondary ice production (Field et al., 2017). Another open question is whether desert dusts serve as a carrier of other more active INP species. For example, it has been shown that fungal ice-nucleating proteins can separate from fungal material and preferentially bind to mineral dust particles (O'Sullivan et al., 2016). In the same vein, a study in the Sahel indicates that biological activity can produce biological ice nucleators, which may become aerosolized (Schnell, 1974b). In addition, it has also been observed that some feldspar minerals can be substantially more active ice nucleators than the K-feldspar defined by Atkinson et al. (2013), but we do not know if these hyperactive feldspars are present in desert soils (Harrison et al., 2016). Through some combination of longer sampling times and

larger volumes of water encompassing a greater number of aerosol particles, it should be possible to increase the sensitivity of INP measurements, as recently demonstrated by (DeMott, Hill, et al., 2015). This might allow the measurement of INP concentrations at temperatures pertinent to secondary ice production. Nevertheless, the recent measurements reported by Welti et al. (2017) suggest that in this region the INP concentration are extremely low in the Hallett-Mossop regime, consistent with the K-feldspar-based model prediction.

Overall, we have quantified the INP spectrum between −25 and −10°C for atmospheric aerosol rich in desert dust, which was sampled within several days' transport from the African source regions. We also demonstrate that laboratory-based parameterizations of ice nucleation by desert dust can reproduce the observed values within about 1 to 2 orders of magnitude. However, significant open questions remain, not least the identity and concentration of INPs at temperatures warmer than −10°C, what causes the discrepancies between the different desert dust INP parameterizations, and also how desert dust INPs are processed when subject to long range transport.

References

Andreae, M. O., Elbert, W., Gabriel, R., Johnson, D. W., Osborne, S., & Wood, R. (2000). Soluble ion chemistry of the atmospheric aerosol and SO2 concentrations over the eastern North Atlantic during ACE-2. *Tellus Series B: Chemical and Physical Meteorology*, *52*(4), 1066–1087. https://doi.org/10.1034/j.1600-0889.2000.00105.x

Atkinson, J. D., Murray, B. J., Woodhouse, M. T., Whale, T. F., Baustian, K. J., Carslaw, K. S., … Malkin, T. L. (2013). The importance of feldspar for ice nucleation by mineral dust in mixed-phase clouds. *Nature*, *498*(7454), 355–358. https://doi.org/10.1038/nature12278

Augustin-Bauditz, S., Wex, H., Kanter, S., Ebert, M., Niedermeier, D., Stolz, F., … Stratmann, F. (2014). The immersion mode ice nucleation behavior of mineral dusts: A comparison of different pure and surface modified dusts. *Geophysical Research Letters*, *41*, 7375–7382. https://doi.org/10.1002/2014GL061317

Baumgardner, D., & Huebert, B. (1993). The airborne aerosol inlet workshop: Meeting report. *Journal of Aerosol Science*, *24*(6), 835–846. https://doi.org/10.1016/0021-8502(93)90050-J

Baustian, K. J., Cziczo, D. J., Wise, M. E., Pratt, K. A., Kulkarni, G., Hallar, A. G., & Tolbert, M. A. (2012). Importance of aerosol composition, mixing state, and morphology for heterogeneous ice nucleation: A combined field and laboratory approach. *Journal of Geophysical Research*, *117*, D06217. https://doi.org/10.1029/2011JD016784

Beard, K. V. (1992). Ice initiation in warm-base convective clouds: An assessment of microphysical mechanisms. *Atmospheric Research*, *28*(2), 125–152. https://doi.org/10.1016/0169-8095(92)90024-5

Boose, Y., Kanji, Z. A., Kohn, M., Sierau, B., Zipori, A., Crawford, I., … Lohmann, U. (2016). Ice-nucleating particle measurements at 241 K during winter months at 3580 m MSL in the Swiss Alps. *Journal of the Atmospheric Sciences*, *73*(5), 2203–2228. https://doi.org/10.1175/jas-d-15-0236.1

Boose, Y., Sierau, B., García, M. I., Rodríguez, S., Alastuey, A., Linke, C., … Lohmann, U. (2016). Ice-nucleating particles in the Saharan air layer. *Atmospheric Chemistry and Physics*, *16*(14), 9067–9087. https://doi.org/10.5194/acp-16-9067-2016

Boose, Y., Welti, A., Atkinson, J., Ramelli, F., Danielczok, A., Bingemer, H. G., … Lohmann, U. (2016). Heterogeneous ice nucleation on dust particles sourced from nine deserts worldwide—Part 1: Immersion freezing. *Atmospheric Chemistry and Physics*, *16*(23), 15075–15095. https://doi.org/10.5194/acp-16-15075-2016

Chou, C., Formenti, P., Maille, M., Ausset, P., Helas, G., Harrison, M., & Osborne, S. (2008). Size distribution, shape, and composition of mineral dust aerosols collected during the African monsoon multidisciplinary analysis special observation period 0: Dust and biomass-burning experiment field campaign in Niger, January 2006. *Journal of Geophysical Research*, *113*, D00C10. https://doi.org/10.1029/2008JD009897

Chou, C., Stetzer, O., Weingartner, E., Jurányi, Z., Kanji, Z. A., & Lohmann, U. (2011). Ice nuclei properties within a Saharan dust event at the Jungfraujoch in the Swiss Alps. *Atmospheric Chemistry and Physics*, *11*(10), 4725–4738. https://doi.org/10.5194/acp-11-4725-2011

Conen, F., Rodríguez, S., Hülin, C., Henne, S., Herrmann, E., Bukowiecki, N., & Alewell, C. (2015). Atmospheric ice nuclei at the high-altitude observatory Jungfraujoch, Switzerland. *Tellus Series B: Chemical and Physical Meteorology*, *67*(1), 25014. https://doi.org/10.3402/tellusb.v67.25014

Connolly, P. J., Möhler, O., Field, P. R., Saathoff, H., Burgess, R., Choularton, T., & Gallagher, M. (2009). Studies of heterogeneous freezing by three different desert dust samples. *Atmospheric Chemistry and Physics*, *9*(8), 2805–2824. https://doi.org/10.5194/acp-9-2805-2009

Crawford, I., Bower, K. N., Choularton, T. W., Dearden, C., Crosier, J., Westbrook, C., … Blyth, A. (2012). Ice formation and development in aged, wintertime cumulus over the UK: Observations and modelling. *Atmospheric Chemistry and Physics*, *12*(11), 4963–4985. https://doi.org/10.5194/acp-12-4963-2012

Cziczo, D. J., Froyd, K. D., Hoose, C., Jensen, E. J., Diao, M., Zondlo, M. A., … Murphy, D. M. (2013). Clarifying the dominant sources and mechanisms of cirrus cloud formation. *Science*, *340*(6138), 1320–1324. https://doi.org/10.1126/science.1234145

DeMott, P. J. (1995). Quantitative descriptions of ice formation mechanisms of silver iodide-type aerosols. *Atmospheric Research*, *38*(1-4), 63–99. https://doi.org/10.1016/0169-8095(94)00088-U

DeMott, P. J., Hill, T. C. J., McCluskey, C. S., Prather, K. A., Collins, D. B., Sullivan, R. C., … Franc, G. D. (2015). Sea spray aerosol as a unique source of ice-nucleating particles. *Proceedings of the National Academy of Sciences of the United States of America*, *113*(21), 5797–5803. https://doi.org/10.1073/pnas.1514034112

DeMott, P. J., Prenni, A. J., McMeeking, G. R., Sullivan, R. C., Petters, M. D., Tobo, Y., … Kreidenweis, S. M. (2015). Integrating laboratory and field data to quantify the immersion freezing ice nucleation activity of mineral dust particles. *Atmospheric Chemistry and Physics*, *15*(1), 393–409. https://doi.org/10.5194/acp-15-393-2015

DeMott, P. J., Sassen, K., Poellot, M. R., Baumgardner, D., Rogers, D. C., Brooks, S. D., … Kreidenweis, S. M. (2003). African dust aerosols as atmospheric ice nuclei. *Geophysical Research Letters*, *30*(14), 1732. https://doi.org/10.1029/2003GL017410

Field, P. R., Lawson, R. P., Brown, P. R. A., Lloyd, G., Westbrook, C., Moisseev, D., … Sullivan, S. (2017). Secondary ice production: Current state of the science and recommendations for the future. *Meteorological Monographs*, *58*, 7.1–7.20. https://doi.org/10.1175/amsmonographs-d-16-0014.1

Formenti, P., Rajot, J. L., Desboeufs, K., Caquineau, S., Chevaillier, S., Nava, S., … Highwood, E. (2008). Regional variability of the composition of mineral dust from western Africa: Results from the AMMA SOP0/DABEX and DODO field campaigns. *Journal of Geophysical Research*, *113*, D00C13. https://doi.org/10.1029/2008JD009903

Formenti, P., Rajot, J. L., Desboeufs, K., Said, F., Grand, N., Chevaillier, S., & Schmechtig, C. (2011). Airborne observations of mineral dust over western Africa in the summer monsoon season: Spatial and vertical variability of physico-chemical and optical properties. *Atmospheric Chemistry and Physics*, *11*(13), 6387–6410. https://doi.org/10.5194/acp-11-6387-2011

Glaccum, R. A., & Prospero, J. M. (1980). Saharan aerosols over the tropical north-Atlantic - mineralogy. *Marine Geology*, *37*(3-4), 295–321. https://doi.org/10.1016/0025-3227(80)90107-3

Hand, V. L., Capes, G., Vaughan, D. J., Formenti, P., Haywood, J. M., & Coe, H. (2010). Evidence of internal mixing of African dust and biomass burning particles by individual particle analysis using electron beam techniques. *Journal of Geophysical Research*, *115*, D13301. https://doi.org/10.1029/2009JD012938

Harrison, A. D., Whale, T. F., Carpenter, M. A., Holden, M. A., Neve, L., O'Sullivan, D., … Murray, B. J. (2016). Not all feldspars are equal: A survey of ice-nucleating properties across the feldspar group of minerals. *Atmospheric Chemistry and Physics*, *16*(17), 10,927–10,940. https://doi.org/10.5194/acp-16-10927-2016

Hiranuma, N., Augustin-Bauditz, S., Bingemer, H., Budke, C., Curtius, J., Danielczok, A., … Yamashita, K. (2015). A comprehensive laboratory study on the immersion freezing behavior of illite NX particles: A comparison of 17 ice nucleation measurement techniques. *Atmospheric Chemistry and Physics*, *15*(5), 2489–2518. https://doi.org/10.5194/acp-15-2489-2015

Hoose, C., Kristjánsson, J. E., Chen, J.-P., & Hazra, A. (2010). A classical-theory-based parameterization of heterogeneous ice nucleation by mineral dust, soot, and biological particles in a global climate model. *Journal of the Atmospheric Sciences*, *67*(8), 2483–2503. https://doi.org/10.1175/2010jas3425.1

Huang, Y., Blyth, A. M., Brown, P. R. A., Choularton, T. W., & Cui, Z. (2017). Factors controlling secondary ice production in cumulus clouds. *Quarterly Journal of the Royal Meteorological Society*, *143*(703), 1021–1031. https://doi.org/10.1002/qj.2987

Johnson, B., Turnbull, K., Brown, P., Burgess, R., Dorsey, J., Baran, A. J., … Rosenberg, P. (2012). In situ observations of volcanic ash clouds from the FAAM aircraft during the eruption of Eyjafjallajökull in 2010. *Journal of Geophysical Research*, *117*, D00U24. https://doi.org/10.1029/2011JD016760

Kamphus, M., Ettner-Mahl, M., Klimach, T., Drewnick, F., Keller, L., Cziczo, D. J., … Curtius, J. (2010). Chemical composition of ambient aerosol, ice residues and cloud droplet residues in mixed-phase clouds: Single particle analysis during the Cloud and Aerosol Characterization Experiment (CLACE 6). *Atmospheric Chemistry and Physics*, *10*(16), 8077–8095. https://doi.org/10.5194/acp-10-8077-2010

Kaufman, Y. J., Koren, I., Remer, L. A., Tanré, D., Ginoux, P., & Fan, S. (2005). Dust transport and deposition observed from the Terra-Moderate Resolution Imaging Spectroradiometer (MODIS) spacecraft over the Atlantic Ocean. *Journal of Geophysical Research*, *110*, D10S12. https://doi.org/10.1029/2003JD004436

Kaufmann, L., Marcolli, C., Hofer, J., Pinti, V., Hoyle, C. R., & Peter, T. (2016). Ice nucleation efficiency of natural dust samples in the immersion mode. *Atmospheric Chemistry and Physics*, *16*(17), 11,177–11,206. https://doi.org/10.5194/acp-16-11177-2016

Klein, H., Nickovic, S., Haunold, W., Bundke, U., Nillius, B., Ebert, M., … Bingemer, H. (2010). Saharan dust and ice nuclei over Central Europe. *Atmospheric Chemistry and Physics*, *10*(21), 10,211–10,221. https://doi.org/10.5194/acp-10-10211-2010

Knippertz, P., & Todd, M. C. (2012). Mineral dust aerosols over the Sahara: Meteorological controls on emission and transport and implications for modeling. *Reviews of Geophysics*, *50*, RG1007. https://doi.org/10.1029/2011RG000362

McCoy, D. T., Hartmann, D. L., Zelinka, M. D., Ceppi, P., & Grosvenor, D. P. (2015). Mixed-phase cloud physics and Southern Ocean cloud feedback in climate models. *Journal of Geophysical Research: Atmospheres*, *120*, 9539–9554. https://doi.org/10.1002/2015JD023603

Murray, B. J., O'Sullivan, D., Atkinson, J. D., & Webb, M. E. (2012). Ice nucleation by particles immersed in supercooled cloud droplets. *Chemical Society Reviews*, *41*(19), 6519–6554. https://doi.org/10.1039/c2cs35200a

Nickovic, S., Vukovic, A., Vujadinovic, M., Djurdjevic, V., & Pejanovic, G. (2012). Technical note: High-resolution mineralogical database of dust-productive soils for atmospheric dust modeling. *Atmospheric Chemistry and Physics*, *12*(2), 845–855. https://doi.org/10.5194/acp-12-845-2012

Niedermeier, D., Augustin-Bauditz, S., Hartmann, S., Wex, H., Ignatius, K., & Stratmann, F. (2015). Can we define an asymptotic value for the ice active surface site density for heterogeneous ice nucleation? *Journal of Geophysical Research: Atmospheres*, *120*, 5036–5046. https://doi.org/10.1002/2014JD022814

Niemand, M., Möhler, O., Vogel, B., Vogel, H., Hoose, C., Connolly, P., … Leisner, T. (2012). A particle-surface-area-based parameterization of immersion freezing on desert dust particles. *Journal of the Atmospheric Sciences*, *69*(10), 3077–3092. https://doi.org/10.1175/jas-d-11-0249.1

O'Sullivan, D., Murray, B. J., Malkin, T. L., Whale, T. F., Umo, N. S., Atkinson, J. D., … Webb, M. E. (2014). Ice nucleation by fertile soil dusts: Relative importance of mineral and biogenic components. *Atmospheric Chemistry and Physics*, *14*(4), 1853–1867. https://doi.org/10.5194/acp-14-1853-2014

O'Sullivan, D., Murray, B. J., Ross, J. F., & Webb, M. E. (2016). The adsorption of fungal ice-nucleating proteins on mineral dusts: A terrestrial reservoir of atmospheric ice-nucleating particles. *Atmospheric Chemistry and Physics*, *16*(12), 7879–7887. https://doi.org/10.5194/acp-16-7879-2016

Peckhaus, A., Kiselev, A., Hiron, T., Ebert, M., & Leisner, T. (2016). A comparative study of K-rich and Na/Ca-rich feldspar ice-nucleating particles in a nanoliter droplet freezing assay. *Atmospheric Chemistry and Physics*, *16*(18), 11,477–11,496. https://doi.org/10.5194/acp-16-11477-2016

Pratt, K. A., DeMott, P. J., French, J. R., Wang, Z., Westphal, D. L., Heymsfield, A. J., … Prather, K. A. (2009). In situ detection of biological particles in cloud ice-crystals. *Nature Geoscience*, *2*(6), 398–401. https://doi.org/10.1038/ngeo521

Price, H. C., K. J. Baustian, J. B. McQuaid, A. Blyth, K. N. Bower, T. Choularton, … B. J. Murray (2017). Datasets associated with 'atmospheric ice-nucleating particles in the dusty tropical Atlantic', Univ. of Leeds, 2017. https://doi.org/10.5518/302

Prospero, J. M., Ginoux, P., Torres, O., Nicholson, S. E., & Gill, T. E. (2002). Environmental characterization of global sources of atmospheric soil dust identified with the NIMBUS 7 Total Ozone Mapping Spectrometer (TOMS) absorbing aerosol product. *Reviews of Geophysics*, *40*(1), 1002. https://doi.org/10.1029/2000RG000095

Pruppacher, H. R., & Klett, J. D. (1997). *Microphysics of Clouds and Precipitation*, (2nd ed.). Dordrecht: Kluwer Academic.

Rangno, A. L., & Hobbs, P. V. (2005). Microstructures and precipitation development in cumulus and small cumulonimbus clouds over the warm pool of the tropical Pacific Ocean. *Quarterly Journal of the Royal Meteorological Society*, *131*(606), 639–673. https://doi.org/10.1256/qj.04.13

Richardson, M. S., DeMott, P. J., Kreidenweis, S. M., Cziczo, D. J., Dunlea, E. J., Jimenez, J. L., … Lersch, T. L. (2007). Measurements of heterogeneous ice nuclei in the western United States in springtime and their relation to aerosol characteristics. *Journal of Geophysical Research*, *112*, D02209. https://doi.org/10.1029/2006JD007500

Ridley, D. A., Heald, C. L., & Ford, B. (2012). North African dust export and deposition: A satellite and model perspective. *Journal of Geophysical Research*, *117*, D02202. https://doi.org/10.1029/2011JD016794

Rosenberg, P. D., Dean, A. R., Williams, P. I., Dorsey, J. R., Minikin, A., Pickering, M. A., & Petzold, A. (2012). Particle sizing calibration with refractive index correction for light scattering optical particle counters and impacts upon PCASP and CDP data collected during the Fennec campaign. *Atmospheric Measurement Techniques*, *5*(5), 1147–1163. https://doi.org/10.5194/amt-5-1147-2012

Schnell, R. C. (1974a). *Biogenic and inorganic sources for ice nuclei in the drought-stricken areas of the Sahel*. New York: Rockerfeller Foundation.

Schnell, R. C. (1974b). Biogenic sources of atmospheric ice nuclei. *Bulletin of the American Meteorological Society*, *55*(6), 670–670.

Schnell, R. C. (1982). Aiborne ice nucleus measurements around the Hawaiian-Islands. *Journal of Geophysical Research*, *87*, 8886–8890. https://doi.org/10.1029/JC087iC11p08886

Soo, J.-C., Monaghan, K., Lee, T., Kashon, M., & Harper, M. (2016). Air sampling filtration media: Collection efficiency for respirable size-selective sampling. *Aerosol Science and Technology*, *50*(1), 76–87. https://doi.org/10.1080/02786826.2015.1128525

Stein, A. F., Draxler, R. R., Rolph, G. D., Stunder, B. J. B., Cohen, M. D., & Ngan, F. (2015). NOAA's HYSPLIT atmospheric transport and dispersion modeling system. *Bulletin of the American Meteorological Society*, *96*(12), 2059–2077. https://doi.org/10.1175/bams-d-14-00110.1

Tan, I., Storelvmo, T., & Zelinka, M. D. (2016). Observational constraints on mixed-phase clouds imply higher climate sensitivity. *Science*, *352*(6282), 224–227. https://doi.org/10.1126/science.aad5300

Twohy, C. H. (2014). Measurements of Saharan dust in convective clouds Over the tropical eastern Atlantic Ocean. *Journal of the Atmospheric Sciences*, *72*(1), 75–81. https://doi.org/10.1175/JAS-D-14-0133.1

Ullrich, R., Hoose, C., Möhler, O., Niemand, M., Wagner, R., Höhler, K., … Leisner, T. (2017). A new ice nucleation active site parameterization for desert dust and soot. *Journal of the Atmospheric Sciences*, *74*(3), 699–717. https://doi.org/10.1175/jas-d-16-0074.1

Vali, G. (1971). Quantitative evaluation of experimental results and the heterogeneous freezing nucleation of supercooled liquids. *Journal of the Atmospheric Sciences*, *28*(3), 402–409. https://doi.org/10.1175/1520-0469(1971)028%3C0402:qeoera%3E2.0.co;2

Vergara-Temprado, J., Murray, B. J., Wilson, T. W., O'Sullivan, D., Browse, J., Pringle, K. J., … Carslaw, K. S. (2017). Contribution of feldspar and marine organic aerosols to global ice-nucleating particle concentrations. *Atmospheric Chemistry and Physics*, *17*(5), 3637–3658. https://doi.org/10.5194/acp-17-3637-2017

Welti, A., Müller, K., Fleming, Z. L., & Stratmann, F. (2017). Concentration and variability of ice nuclei in the subtropic, maritime boundary layer. *Atmospheric Chemistry and Physics Discussions*, *2017*, 1–18. https://doi.org/10.5194/acp-2017-783

Wex, H., DeMott, P. J., Tobo, Y., Hartmann, S., Rösch, M., Clauss, T., … Stratmann, F. (2014). Kaolinite particles as ice nuclei: Learning from the use of different kaolinite samples and different coatings. *Atmospheric Chemistry and Physics*, *14*(11), 5529–5546. https://doi.org/10.5194/acp-14-5529-2014

Whale, T. F., Holden, M. A., Kulak, A. N., Kim, Y.-Y., Meldrum, F. C., Christenson, H. K., & Murray, B. J. (2017). The role of phase separation and related topography in the exceptional ice-nucleating ability of alkali feldspars. *Physical Chemistry Chemical Physics*, *19*(46), 31186–31193. https://doi.org/10.1039/C7CP04898J

Whale, T. F., Murray, B. J., O'Sullivan, D., Wilson, T. W., Umo, N. S., Baustian, K. J., … Morris, G. J. (2015). A technique for quantifying heterogeneous ice nucleation in microlitre supercooled water droplets. *Atmospheric Measurement Techniques*, *8*(6), 2437–2447. https://doi.org/10.5194/amt-8-2437-2015

Wiacek, A., Peter, T., & Lohmann, U. (2010). The potential influence of Asian and African mineral dust on ice, mixed-phase and liquid water clouds. *Atmospheric Chemistry and Physics*, *10*(18), 8649–8667. https://doi.org/10.5194/acp-10-8649-2010

Wilson, T. W., Ladino, L. A., Alpert, P. A., Breckels, M. N., Brooks, I. M., Browse, J., … Murray, B. J. (2015). A marine biogenic source of atmospheric ice-nucleating particles. *Nature*, *525*(7568), 234–238. https://doi.org/10.1038/nature14986

Young, G., Jones, H. M., Darbyshire, E., Baustian, K. J., McQuaid, J. B., Bower, K. N., … Choularton, T. W. (2016). Size-segregated compositional analysis of aerosol particles collected in the European Arctic during the ACCACIA campaign. *Atmospheric Chemistry and Physics*, *16*(6), 4063–4079. https://doi.org/10.5194/acp-16-4063-2016

Zolles, T., Burkart, J., Hausler, T., Pummer, B., Hitzenberger, R., & Grothe, H. (2015). Identification of ice nucleation active sites on feldspar dust particles. *Journal of Physical Chemistry A*, *119*(11), 2692–2700. https://doi.org/10.1021/jp509839x